

# Low power ultra-broadband terahertz sideband generation in bi-layer graphene

J. A. Crosse<sup>1</sup>, Xiaodong Xu<sup>2</sup>, Mark S. Sherwin<sup>3</sup>, & R. B. Liu<sup>1\*</sup>

<sup>1</sup> *Department of Physics and Center for Quantum Coherence, The Chinese University of Hong Kong, Shatin, New Territories, Hong Kong, China.*

<sup>2</sup> *Department of Physics, Department of Material Science and Engineering, University of Washington, Seattle, Washington 98195, USA.*

<sup>3</sup> *Department of Physics and the Institute for Terahertz Science and Technology, University of California at Santa Barbara, Santa Barbara, California 93106, USA.*

\* e-mail: [rbliu@phy.cuhk.edu.hk](mailto:rbliu@phy.cuhk.edu.hk)

**In a semiconductor, an electron-hole pair, created by a weak optical laser and accelerated by an intense terahertz (THz) field, can recombine to emit light in a broad frequency comb evenly spaced by twice the THz frequency [1, 2]. Such high-order THz sideband generation (HSG) is not only of fundamental interest, as an example of extreme nonlinear optics in condensed matter systems, but also of technological importance as a mechanism for ultrafast electro-optical modulation - a crucial ingredient in Tbit/sec rate optical communication. However, a broad HSG spectrum, or, equivalently, a deep electro-optical modulation in the time-domain, requires intense THz fields that are only available through large scale installations such as synchrotrons or free-electron lasers [3, 4]. The need for such large field strengths precludes the practical use of HSG. Here we report on the discovery that bi-layer graphene [5-7] is a much more efficient material for HSG than conventional semiconductors. We find that a THz field of strength 1 kV/cm can produce an HSG spectrum of about 30 THz in the telecom waveband, 100 times broader than in GaAs (or, equivalently, a comparable**

**bandwidth in GaAs would require THz field intensities that are 100 times stronger). These remarkable features make it possible to realise HSG with a much weaker THz laser, which enables desktop electro-optical modulation at THz frequencies, facilitating ultrafast optical communications.**

The optical modulation that occurs when an intense light field interacts with matter has a wide range of applications, from molecular imaging [8, 9] to soft X-ray generation [10-12] and potential applications in all-optical signal processing. The well-known atomic process of high-harmonic generation (HHG) [13] is an example of such a process.

HHG can be understood with a three step model. In the first step an electron is ionized from an atom by an intense field. In the second, the ionised electron is accelerated by the field along a closed orbit, returning to the ion at a later time with a higher energy. Finally, the electron recombines with the ion releasing a photon which is an odd harmonic of the original field [Fig. 1(a)]. One important feature of the process is its 'non-perturbative' nature, which results in a 'plateau-like' spectrum where the intensity of the harmonics remain approximately constant up to a cutoff frequency of  $I_p + 3.17U_p$  (where  $I_p$  is the atom binding energy and  $U_p = \frac{e^2 E^2}{4m_e \omega^2}$  is the ponderomotive energy with  $E$  and  $\omega$  the strength and angular frequency of the light field and  $e$  and  $m_e$  the charge and mass of the driven electron, respectively), outside of which the harmonic strength decays away exponentially [14-16]. The similar process of HSG can occur in semiconductors [1]. In HSG, a weak optical field promotes a valence band electron to the conduction band, creating an electron-hole pair. The pair is then driven in the band by an intense, THz frequency field. The recombination of the electron-hole pair results in the generation of sidebands in the excitation field spectrum that occur at even harmonics of the THz field. As with HHG, the 'non-perturbative' plateau occurs with a cutoff of  $\Delta + 3.17U_p$  (where  $\Delta$  is the detuning of laser from the band gap of the

semiconductor and  $U_p = \frac{e^2 E_{THz}^2}{4m_R \omega_{THz}^2}$  is the ponderomotive energy with  $E_{THz}$  and  $\omega_{THz}$  the strength and angular frequency of the THz field and  $m_R$  the electron-hole reduced mass). HSG has a wide range of potential applications but there is a serious technological challenge; HSG requires large THz field strengths. Current experimental observations of HSG have employed THz field amplitudes on the order of  $10 \text{ kVcm}^{-1}$  [2] which, with current technology, are only available through large scale installations such as synchrotrons or free-electron lasers [3, 4]. The need for such large field strengths precludes the use of HSG in optical devices.

Novel materials, such as graphene, offer a potential solution to this problem. The maximum modulation bandwidth is given by the maximum kinetic energy that can be obtained from the THz field by the electron-hole pair. This, in turn, is given by the work done on the electron-hole pair by the THz field,  $\int e E_{THz} v dt$ , which is linearly proportional to their velocity,  $v$ . Electrons in graphene act like massless Dirac electrons and hence have a large initial velocity ( $v_f \approx c/300$ ). Conversely, electrons in conventional parabolic band semiconductors have vanishing initial velocity near the band edge. Hence, graphene's linear dispersion and ballistic electrons offer a significant energy gain, at least at low energies, over the parabolic bands of traditional semiconductor and, therefore, is a promising candidate material for HSG at the low-field intensities which would be suitable for optical device design. In addition, graphene's resonant transition at telecomm frequencies [17], weak uniform absorptive loss [18] and ultrafast optical response [19] make it an ideal candidate for optical communication applications. In fact, it has been demonstrated that graphene, owing to its ultrafast electrical response, is a promising material for ultrafast electro-optical modulation [20].

There are, however, a number of marked differences between HSG in graphene and in conventional semiconductors. In a conventional semiconductor the dominant process by

which HSG occurs is semi-classical; the electron and hole return to the same location to recombine. In graphene, owing to their massless nature, the electron and hole act like photons in that their velocity is fixed at the Fermi velocity. The action of the THz field changes the momentum and energy of the electron and hole but the velocity remains constant. As a result, the electron and hole separate at a constant rate and do not return to the same location [Fig. 1(b)]. However, recent work has shown that sidebands can still be generated if the electron and hole wavefunctions are broad enough to allow significant overlap at the point of maximum classical excursion [21]. It is this ‘quantum’ process that is the dominant mechanism of HSG in graphene.

We show that bi-layer graphene (BLG) is a versatile system for HSG at telecommunication wavelength (1.5  $\mu\text{m}$ ). Instead of monolayer graphene, we consider BLG since a bias field can be applied to the dual layer structure to open a gap at the Dirac point, which avoids excitations of many electron-hole pairs by the THz field (Schwinger instability [22]) [Fig. 2(a)]. Yet the linear dispersion at the telecomm frequencies is maintained in BLG. The low energy band structure of BLG [6, 7] displays four, valley degenerate bands of which the two of lower energy,  $E_v$  and  $E_{v'}$ , are fully occupied valence bands and the two of higher energy,  $E_c$  and  $E_{c'}$ , are fully empty conduction bands [Fig. 2(b)]. With a relatively low intensity THz field and an excitation field in the C-band of the telecomm frequency range only one of the four possible transitions is significant. The major contribution to the spectrum comes from the  $E_v \rightarrow E_c$  transition [labelled (4) in Fig. 2(b)] where both the electron and hole are created in the linear-dispersion region. This is where the initial velocity is highest and hence where the maximum kinetic energy gain can be obtained. The other transitions [labeled (1-3) in Fig. 2(b)] contribute negligibly to the HSG spectrum as either the electron or hole is created in the parabolic-dispersion region or the optical excitation is off resonant or both.

In the following we study the optical spectrum of a THz driven electron-hole pair in biased BLG. We treat the THz-field as a continuous wave of the form,  $\mathbf{F}_{THz}(t) = \mathbf{F}_{THz} \cos \omega_{THz} t$ , which we take to be polarized in the x-direction (Fig. 1a). Similarly, the weak excitation field is taken to be a continuous wave,  $\mathbf{F}_{ex}(t) = \mathbf{F}_{ex} e^{-i\omega_{ex} t}$ . The coupling of the THz field to the material is introduced via the time-dependent canonical momentum by the inclusion of the vector potential  $\mathbf{k} \rightarrow \tilde{\mathbf{k}}(t) = \mathbf{k} + \mathbf{A}_{THz}(t)$  with  $\mathbf{F}_{THz} = -\frac{\partial \mathbf{A}_{THz}(t)}{\partial t}$ . If the excitation field is sufficiently weak one can work in the quasi-equilibrium regime where the depletion of the valence band is negligible. We also note that the large gap induced by the bias field prevents interband transitions caused by the THz field. These facts allow us to work in the single active electron approximation and, hence, ignore electron-electron correlation effects.

We evaluate this system by direct simulation of the time dependent Schrödinger equation for an excitation field of 1.55  $\mu\text{m}$  (194 THz), which is located in the C-band of the telecomm frequencies, and a THz field of frequency 1 THz. The potential induced by the bias voltage on the BLG was set to 0.2 eV, which is achievable with a field of 2  $\text{Vnm}^{-1}$  [23]. The dephasing factor,  $\Gamma$ , is introduced to accounts for various relaxation mechanisms. In monolayer graphene there are three main relaxation mechanisms, namely, carrier-carrier scattering [24, 25], which occurs on tens of femtosecond scale, and carrier-phonon scattering [24, 25] and electron-hole recombination [25], which occurs on the picosecond timescale; we expect similar order of magnitude values for BLG. Since we are working in the single active electron approximation carrier-carrier scattering is essentially absent so the dominant relaxation process is carrier-phonon scattering which has been measured to be  $\approx 600$  fs [24] and hence, we set to the relaxation time,  $\hbar/\Gamma$ , to 658 fs ( $\Gamma=1$  meV) [A detailed discussion of the effect of relaxation rates can be found in Supplementary Information (Fig. S1)]. The sideband spectrum was calculated for a number of THz field strengths, ranging from 1  $\text{kVcm}^{-1}$  to 4

$\text{kVcm}^{-1}$ . Figure 3(a) shows the sideband spectrum for increasing THz field strength. At a THz field strength of  $1 \text{ kVcm}^{-1}$  one can see a plateau, symmetric about the excitation frequency, of width  $\approx 28 \text{ THz}$  [Fig 3(b)]. As one increases the THz field strength the plateau grows linearly reaching a width of about  $108 \text{ THz}$  for a  $4 \text{ kVcm}^{-1}$  field [Fig 3(c)].

The advantages of BLG as a material for HSG can be seen by comparison with conventional semiconductors such as GaAs. In order to obtain a bandwidth of about  $28 \text{ THz}$  with a  $1 \text{ THz}$  frequency field one would need a field strength of nearly  $14 \text{ kVcm}^{-1}$  (i.e., the required THz field intensity for GaAs is  $\sim 200$  times stronger than for the BLG). Another advantage is that BLG has resonant transitions throughout the telecomm frequencies (including all standard band classifications from O-band to U-band, not just the conventional C-band “erbium window”), thus allowing broadband modulation at any frequency in this range. This would mean that BLG based devices could operate optimally over a wide range of frequencies without the need to further tailor the material. Conversely, the GaAs bandgap (which corresponds to a wavelength of  $\sim 0.87 \text{ }\mu\text{m}$ ) is outside the telecomm frequency waveband. Even materials with smaller band gaps (e.g. silicon  $\sim 1.12 \text{ }\mu\text{m}$ , germanium  $\sim 1.85 \text{ }\mu\text{m}$ ) usually need further engineering (either by alloying or via the creation of heterostructures) in order to create a device that is optimally tuned to a particular optical frequency. For exceptionally small band-gap semiconductors (such as InAs  $\sim 3.44 \text{ }\mu\text{m}$ ), a field in the telecomm waveband can also create electron-hole pairs well above the band edge and therefore with high initial velocity. However, the carrier relaxation in such materials, due to the rapid emission of LO phonons (which have energies of tens of meV), would be much faster than in graphene (where the LO phonon energy  $\sim 200 \text{ meV}$  [26]).

To further understand the plateau of HSG in BLG, we compare the theoretical model to the equivalent theory for conventional semiconductors. For a parabolic band material the Schrödinger equation can be solved in a semi-classical approximation to give an expression

for the plateau cutoff  $\Delta + 3.17U_p$  [1, 16]. One can follow a similar procedure to obtain a cutoff law for BLG (see Supplementary Information). The  $E_v$  and  $E_c$  bands can be expanded to first order about the excitation energy

$$E_c[\tilde{\mathbf{k}}(t)] - E_v[\tilde{\mathbf{k}}(t)] \approx E_g + 2\hbar\tilde{v}_{f,vc} \cdot (\tilde{\mathbf{k}}(t) - \mathbf{k}_{ex}). \quad (1)$$

The result is a band structure that resembles a shifted version of monolayer graphene with effective Fermi velocity,  $\tilde{v}_{f,vc}$ . Solving a restricted version of the classical equations of motion for such a system leads to a prediction for the plateau cutoffs of at  $4|\tilde{U}_{p,vc}|$  above and below the excitation frequency, with linear ponderomotive energy  $\tilde{U}_{p,vc} = \frac{e\tilde{v}_{f,vc}|E_{THz}|}{\omega_{THz}}$ . The dashed black line in Fig. 3(a) shows the theoretical prediction of the cutoff. One observes good agreement over the full range of THz field strengths simulated. Similarly, the black arrows in Figs. 3(b) and (c) mark the theoretical cutoff given by the  $4|\tilde{U}_{p,vc}|$  cutoff law. Figure 3(b) shows that at low field strengths the cutoff law is in good agreement with the numerical results. Figure 3(c) shows that although the cutoff law correctly predicts the high end cutoff it over-estimates the low end cutoff. The reason for this is that as the bands move towards the Dirac point they deviate from linear and, hence, the electron and hole have lower velocities. This leads to the discrepancy observed in Fig. 3(c).

The results of this study suggest that biased BLG can provide ultra-broad HSG and, hence, ultrafast modulation of an optical field at THz field strengths low enough for table top sources to be used [27-29]. These results open up the way for ultrafast, HSG based, optical devices, which, coupled with the remarkable properties of BLG, marks a step towards realising all optical broadband modulation and optical communication at the Tbit/sec rate.

## Methods

The electron-hole pair wavefunction,  $P_{\sigma,\lambda}(\tilde{\mathbf{k}}, t) = \langle \hat{e}_{\sigma,\lambda}(\tilde{\mathbf{k}}, t) \hat{h}_{\sigma,\lambda}(\tilde{\mathbf{k}}, t) \rangle$ , where  $\lambda$  and  $\sigma$  are the spin and valley indices respectively, was computed using the time-dependent Schrödinger equation

$$i\hbar \frac{\partial}{\partial t} P_{\sigma,\lambda}(\tilde{\mathbf{k}}, t) = \Delta E[\tilde{\mathbf{k}}(t)] P_{\sigma,\lambda}(\tilde{\mathbf{k}}, t) + i \mathbf{d}_{vc}[\tilde{\mathbf{k}}(t)] \cdot \mathbf{F}_{ex}(t), \quad (2)$$

with

$$\Delta E[\tilde{\mathbf{k}}(t)] = E_c[\tilde{\mathbf{k}}(t)] - E_v[\tilde{\mathbf{k}}(t)] - \hbar\omega_{ex} - i\Gamma + i\{\mathbf{A}_c^*[\tilde{\mathbf{k}}(t)] + \mathbf{A}_v[\tilde{\mathbf{k}}(t)]\} \cdot \mathbf{F}_{THz}(t). \quad (3)$$

Here,  $E_c[\tilde{\mathbf{k}}(t)]$  and  $E_v[\tilde{\mathbf{k}}(t)]$  are the instantaneous valence and conduction band energies, which can be derived using a tight-binding method with nearest neighbour hopping [6, 7].

The time-dependent canonical momentum is given by  $\tilde{\mathbf{k}}(t) = \left( \mathbf{k} - \frac{e}{\hbar} \int dt' \mathbf{F}_{THz}(t') \right)$ , and  $\mathbf{d}_{vc}[\tilde{\mathbf{k}}(t)] = e \langle v, \tilde{\mathbf{k}}(t) | \nabla_{\mathbf{k}} | c, \tilde{\mathbf{k}}(t) \rangle$  and  $\mathbf{A}_i[\tilde{\mathbf{k}}(t)] = e \langle i, \tilde{\mathbf{k}}(t) | \nabla_{\mathbf{k}} | i, \tilde{\mathbf{k}}(t) \rangle$  are the interband dipole moment and Berry connection terms [30], the latter of which is required to preserve gauge invariance. As the driving of the electrons is linear (as opposed to closed orbits) the contribution of the Berry connection term is negligible (see Supplementary Information).  $\Gamma$  is a phenomenological dephasing rate that accounts for various relaxation mechanisms. Finally,  $\lambda$  and  $\sigma$  are the spin and valley indices respectively. For the sake of simplicity, we have not included the Coulomb interaction. This is justified by the condition that the resonant excitation is taken to be far from the band edge and hence off-resonant with the bound state excitations. Furthermore, at such high quasi-momenta, the kinetic term in the Hamiltonian will dominate. Equation (2) was evaluated directly using standard numerical techniques. The resulting polarization is given by

$$\mathbf{P}(t) = i \langle \hat{\mathbf{d}}_{vc}(t) \rangle = i \sum_{\lambda,\sigma} \int d^3k \mathbf{d}_{vc}^*[\tilde{\mathbf{k}}(t)] P_{\sigma,\lambda}(\tilde{\mathbf{k}}, t), \quad (4)$$

with the sideband spectrum calculated via discrete Fourier transform.

**Full methods and supplementary figures are available online.**



## References

1. Liu, R.-B. and Zhu, B.-F. High-order THz-sideband generation in semiconductors. *Physics of Semiconductors: 28th International Conference on the Physics of Semiconductors ICPS 2006, AIP Conf. Proc.* **893**, 1455 (2007).
2. Zaks, B., Liu, R.-B. and Sherwin, M. Experimental observation of electron-hole recollisions. *Nature* **483**, 580 (2012).
3. Stojanovic N., and Drescher, M. Accelerator- and laser-based sources of high-field terahertz pulses. *J. Phys. B: At. Mol. Opt. Phys.* **46**, 192001 (2013).
4. Williams, G. P., Filling the THz gap – high power sources and applications. *Rep. Prog. Phys.* **69**, 301 (2006).
5. McCann, E., and Koshino, M. The electronic properties of bi-layer graphene. *Rep. Prog. Phys.* **76**, 056503 (2013).
6. McCann, E., Abergel, D. S. L. and Falko, V. I. Electrons in bi-layer graphene. *Solid State Comm.* **143**, 110 (2007).
7. McCann, E., Abergel, D. S. L. and Falko, V. I. The low energy electronic band structure of bi-layer graphene. *Eur. Phys. J. Special Topics* **148**, 91 (2007).
8. Itatani, J., et al. Tomographic imaging of molecular orbitals. *Nature* **432**, 867 (2004).
9. Baker, S. et al. Probing proton dynamics in molecules on an attosecond time scale. *Science* **312**, 424 (2006).
10. Spielmann, Ch., et al. Generation of coherent xrays in the water window using 5-femtosecond laser pulses. *Science* **278**, 661 (1997).
11. Neutze, R., Wouts, R., van der Spoel, D., Weckert, E. and Hajdu, J. Potential for biomolecular imaging with femtosecond X-ray pulses. *Nature* **406**, 752 (2000).
12. Dromey, B., et al. High harmonic generation in the relativistic limit. *Nat. Phys.* **2**, 456 (2006).

13. Joachain, C. J., Kylstra, N. J., and Potvliege, R. M. *Atoms in Intense Laser Fields*, (Cambridge University Press, Cambridge, 2012).
14. Krause, J. L., Schafer, K. J. and Kulander, K. C. High-order harmonic generation from atoms and ions in the high intensity regime. *Phys. Rev. Lett.* **68**, 3535 (1992).
15. Corkum, P. B. Plasma perspective on strong-field multiphoton ionization. *Phys. Rev. Lett.* **71**, 1994 (1993).
16. Lewenstein, M., Balcou, Ph., Ivanov, M. Yu., L'Huillier A., and Corkum, P. B. Theory of high-harmonic generation by low-frequency laser fields. *Phys. Rev. A* **49**, 2117 (1994).
17. Saito, R., Dresselhaus, G. and Dresselhaus, M. S. *Physical Properties of Carbon Nanotubes* (Imperial College Press, 1998).
18. Nair, R. R., et al. Fine structure constant defines visual transparency of graphene. *Science*, **320**, 1308 (2008).
19. Prechtel, L., et al. Time-resolved ultrafast photocurrents and terahertz generation in freely suspended graphene. *Nat. Comm.* **3**, 646 (2012).
20. Liu, M., et al. A graphene-based broadband optical modulator, *Nature* **474**, 64 (2011).
21. Crosse, J. A. and Liu, R.-B. Quantum coherence induced second plateau in high-sideband generation, arXiv:1311.6237 (2013).
22. Allor, D., Cohen, T.D. and McGady, D. A. Schwinger mechanism and graphene, *Phys. Rev. D* **78**, 096009 (2008).
23. Zhang, Y., et al. Direct observation of a widely tunable bandgap in bi-layer graphene. *Nature* **459**, 820 (2009).
24. Sun, D., et al. Current Relaxation due to hot carrier scattering in graphene, *New J. Phys.* **14**, 105012 (2012).
25. George, P. A., et al. Ultrafast optical pump Terahertz-probe spectroscopy of the carrier relaxation and recombination dynamics in epitaxial graphene, *Nano. Lett.* **8**, 4248 (2008).

26. Piscanec, S., Lazzeri, M., Mauri, F. and Ferrari, A. C. Optical phonons of graphene and nanotubes, *Eur. Phys. J. Special Topics* **148**, 159 (2007).
27. Tonouchi, M. Cutting-edge terahertz technology, *Nat. Phot.* **1**, 97 (2007).
28. Edwards, T. J., et al. Compact Source of continuously and widely-tunable terahertz radiation, *Opt. Exp.* **14**, 1582 (2006).
29. Benicewicz, P. K. and Taylor, A. J. Scaling of terahertz radiation from large-aperture biased InP photoconductors, *Opt. Lett.* **18**, 1332 (1997).
30. Yang, F., Xu, X. and Liu, R.-B. Giant Faraday rotation induced by Berry phase in bilayer graphene under strong terahertz fields, arXiv:1307.7987 (2013).

**Acknowledgements** We acknowledge supports from Hong Kong Research Grants Council – General Research Fund Project 401512 and The Chinese University of Hong Kong Focused Investments Scheme.

**Author contributions** R.B.L. conceived the idea and supervised the project. R.B.L., X.D.X., and M.S. designed the device. J.A.C. carried out the theoretical study and numerical calculation. J.A.C. wrote the paper. All authors analysed the data and commented on the manuscript.

**Additional information** The authors declare no competing financial interests. Supplementary information accompanies this paper. Correspondence and requests for materials should be addressed to R.B.L.

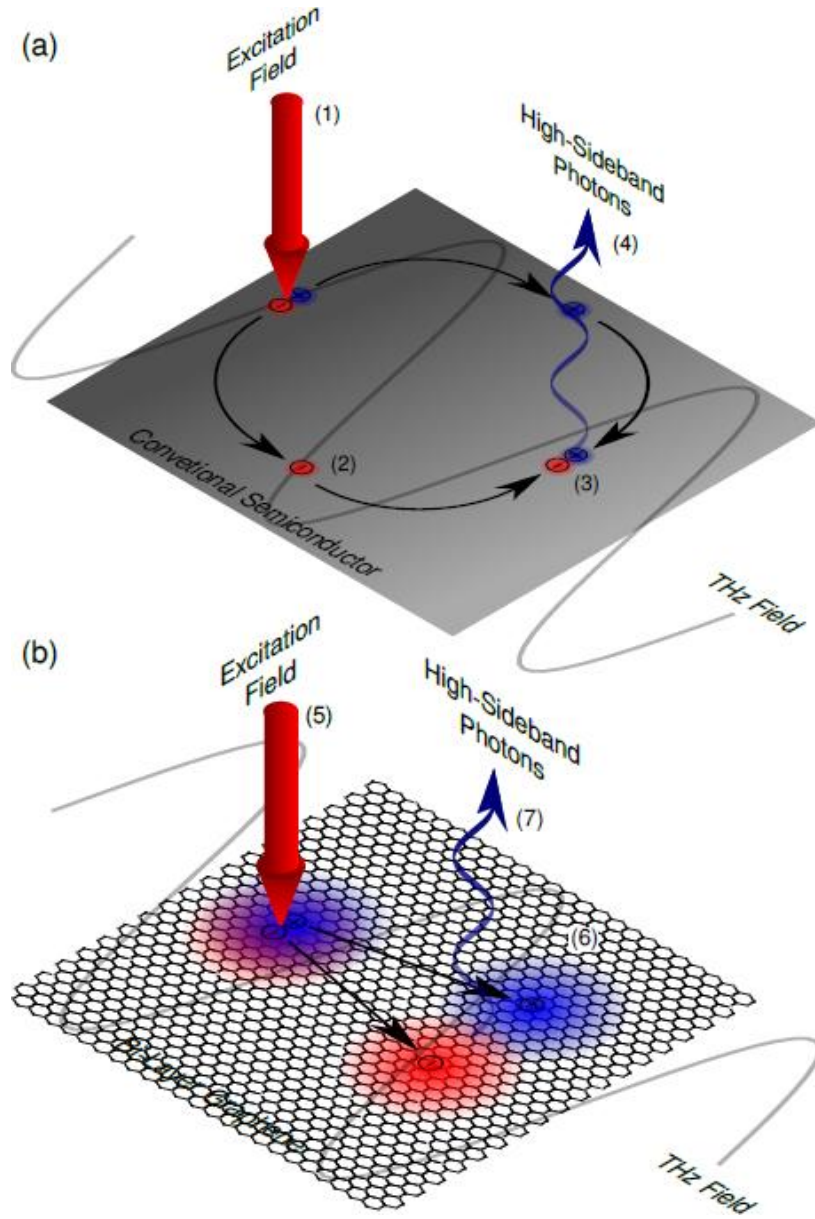


**Figure 1: Schematics of high-sideband generation in conventional semiconductors and in graphene. (a)** In a conventional semiconductor, an electron-hole pair, created by a weak excitation field (1), is accelerated by an intense THz frequency field gaining energy. The electron and hole wavefunctions separate completely (2). The THz field drives the electron and hole back towards each other, recombining (3) and releasing a high-sideband photon (4). **(b)** In graphene, a weak excitation field excites an electron-hole pair (5) which is accelerated in opposite

directions by the THz field (6). As the electron-hole pair has vanishing effective mass the THz alters their energy and momentum but not their velocity. Hence the electron and hole separate at the Fermi Velocity. However, owing to the broad wavefunction of the electron and hole, there is still significant overlap at finite separations and, hence, recombination (and the release of a high-sideband photon) is possible even though the classical locations of the electron and hole do not coincide (7).

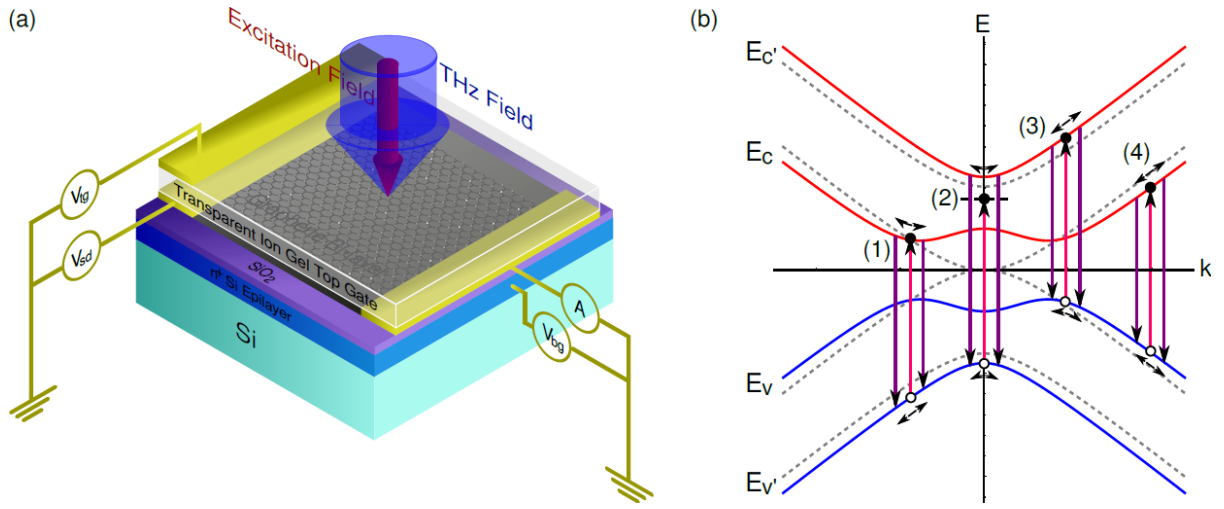


**Figure 2: Device structure and mechanism for high-sideband generation in bi-layer graphene.** (a) Device design for high-sideband generation. A single sheet of BLG is layered on a silicon dioxide substrate and biased via a gate voltage. The top gate is transparent in order to allow the incident THz and optical excitation fields to reach the graphene layer. The  $n^+$  Si epilayer should be thin compared to the penetration depth of the THz field in order to avoid significant reflection. (b) Acceleration of electrons/holes along the energy bands. The grey curves show the band structure for unbiased BLG. The four hyperbolic bands are gapless at the Dirac point rendering the material a semi-metal. The application of a bias field opens a gap at the Dirac point, converting BLG from a semi-metal to a semi-conductor. The  $1.55\mu\text{m}$  excitation field creates electron-hole pairs, via three resonant [(1), (3) and (4)] and one off-resonant transitions (2). These electron hole pairs are then driven in the band, recombining to produce the optical sideband spectrum. The dominant contribution is from the transition between the  $E_v \rightarrow E_c$  (4) which occurs in the linear region of the bands.

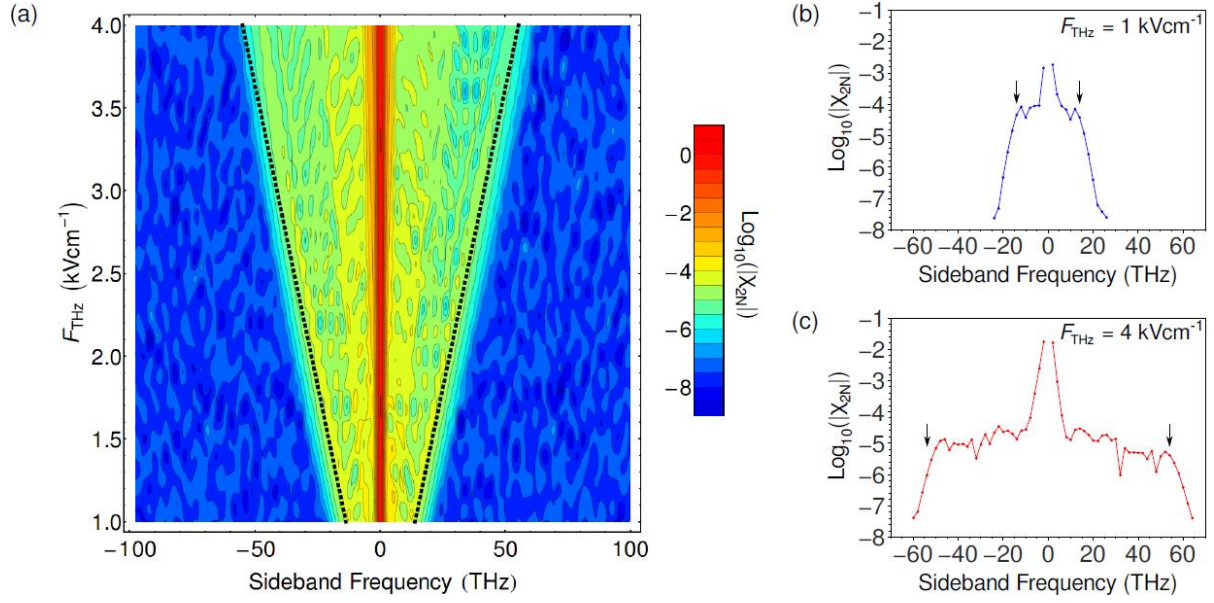


**Figure 3: Sideband spectrum of a THz driven bi-layer graphene. (a)** Contour plot of the sideband spectrum of THz driven BLG for different THz field strengths. The colour map gives the logarithm of the normalized sideband amplitude  $\log_{10}(|X_{2N}|)$ . The dashed black lines give the theoretical sideband cutoffs  $\pm 4U_{p,vc}$ . **(b)** The sideband spectrum for a THz field of frequency 1 THz and strength of  $1 \text{ kVcm}^{-1}$ . **(c)** The sideband spectrum for a THz field of frequency 1 THz and strength  $4 \text{ kVcm}^{-1}$ . The arrows in (b) and (c) mark the location of the theoretical sideband cutoffs,  $\pm 4U_{p,vc}$ .

## SUPPLEMENTARY INFORMATION for

### Low power ultra-broadband terahertz sideband generation in bi-layer graphene

J. A. Crosse<sup>1</sup>, Xiaodong Xu<sup>2</sup>, Mark S. Sherwin<sup>3</sup>, & R. B. Liu<sup>1\*</sup>

<sup>1</sup> *Department of Physics and Center for Quantum Coherence, The Chinese University of Hong Kong, Shatin, New Territories, Hong Kong, China.*

<sup>2</sup> *Department of Material Science and Engineering, University of Washington, Seattle, Washington 98195, USA.*

<sup>3</sup> *Department of Physics and the Institute for Terahertz Science and Technology, University of California at Santa Barbara, Santa Barbara, California 93106, USA.*

\* e-mail: [rbliu@phy.cuhk.edu.hk](mailto:rbliu@phy.cuhk.edu.hk)

#### The band structure of bi-layer graphene

The low energy band structure of bi-layer graphene (BLG) can be derived via a tight-binding method with nearest neighbour hopping [6, 7]. This results in two Hamiltonians, one each for the + and – valleys

$$H_{\pm} = \begin{pmatrix} V & v_f k_{\mp} & 0 & 0 \\ v_f k_{\pm} & V & 2\gamma & 0 \\ 0 & 2\gamma & -V & v_f k_{\mp} \\ 0 & 0 & v_f k_{\pm} & -V \end{pmatrix}, \quad (\text{S1})$$

where  $k_{\pm} = k_x \pm ik_y$ ,  $v_f = -6.462 \frac{eV\text{\AA}}{\hbar}$  is the Fermi velocity [31, 32] (from numerical parameters given in [17]),  $\gamma = 0.202 \text{ eV}$  is the interlayer hopping [33] (Note that  $\gamma$  has been rescaled by a factor of  $\frac{1}{2}$  compared with the value in [33]) and  $V$  is the bias field applied to each layer (which, in the main text, is taken to be 0.2eV). Diagonalization leads to four spin and valley degenerate eigenbands centred about the Fermi energy



$$\begin{aligned}
E_{c'}(\mathbf{k}) &= \sqrt{v_f^2 |\mathbf{k}|^2 + 2\gamma^2 + V^2 + 2\sqrt{v_f^2 |\mathbf{k}|^2 (\gamma^2 + V^2) + \gamma^4}}, \\
E_c(\mathbf{k}) &= \sqrt{v_f^2 |\mathbf{k}|^2 + 2\gamma^2 + V^2 - 2\sqrt{v_f^2 |\mathbf{k}|^2 (\gamma^2 + V^2) + \gamma^4}}, \\
E_v(\mathbf{k}) &= -\sqrt{v_f^2 |\mathbf{k}|^2 + 2\gamma^2 + V^2 - 2\sqrt{v_f^2 |\mathbf{k}|^2 (\gamma^2 + V^2) + \gamma^4}}, \\
E_{v'}(\mathbf{k}) &= -\sqrt{v_f^2 |\mathbf{k}|^2 + 2\gamma^2 + V^2 + 2\sqrt{v_f^2 |\mathbf{k}|^2 (\gamma^2 + V^2) + \gamma^4}}.
\end{aligned} \tag{S2}$$

In the absence of the bias field, the band structure consists of four hyperbolic bands with a gapless transition at the two Dirac points. As with monolayer graphene (MLG), the Fermi surface passes through the Dirac points resulting in two fully filled valence bands and two fully empty conduction bands. The application of a bias field shifts the bands, converting BLG from a gapless semi-metal to a gapped semiconductor. For equal and opposite potentials applied to each of the two graphene layers the Fermi level is unchanged in relation to the bands and remains in the gap [See Fig. 2(b)].

### The Berry connection

One important difference between BLG and traditional semiconductors is the appearance of the Berry connection,  $A_i[\tilde{\mathbf{k}}(t)] = e\langle i, \tilde{\mathbf{k}}(t) | \nabla_{\mathbf{k}} | i, \tilde{\mathbf{k}}(t) \rangle$ , where the index,  $i$ , refers to one of the four energy bands. This term is a result of the non-trivial geometry of the bands and, as the dipole moments are dependent on  $\mathbf{k}$ , is required to maintain the gauge invariance of the optical response. For circularly a polarized THz field, where trajectories of the driven electrons perform elliptic orbits around the Dirac point, or for electrons in a magnetic field, which undergo cyclotron orbits, the geometric phase leads to a number of non-trivial effects

[30, 34-36]. However, in the present case, with a linearly polarized THz field in the absence of a magnetic field, the contribution from the geometric phase vanishes.

### Derivation of the cutoff law

The sideband spectrum can be found from the Fourier transform of the polarization, which is given by the expectation value of the dipole moment operator [Eq. (4) in the main text], which in turn, can be computed from the electron-hole pair wave function whose time evolution is given by Eq. (2) in the main text. The formal solution to Eq. (2) leads to a sideband spectrum

$$\mathbf{P}(\omega) = -\frac{2i}{\pi\hbar} \int d^3k \int dt \int_0^\infty d\tau \mathbf{d}_{vc}^*[\tilde{\mathbf{k}}(t)] e^{iS(\tilde{\mathbf{k}}, t, \tau)} \mathbf{d}_{vc}^*[\tilde{\mathbf{k}}(t)] \cdot \mathbf{F}_{ex}(t), \quad (\text{S3})$$

with the quasi-classical action

$$S(\tilde{\mathbf{k}}, t, \tau) = -\frac{1}{\hbar} \int_{t-\tau}^t dt'' \Delta E[\tilde{\mathbf{k}}(t)] + \omega t, \quad (\text{S4})$$

where  $\Delta E[\tilde{\mathbf{k}}(t)]$  is given in Eq. (3) in the main text. Note that an extra factor of four appears in Eq. (S3) as a result of the spin and valley degeneracy of the bands as one obtains equal contributions from each. For parabolic band semiconductors the expression in Eq. (S3) leads to Gaussian-like integrals which can be evaluated via a saddle-point or stationary phase approximation [1, 16, 37]. Since the BLG bands are not of quadratic form they do not lend themselves to the traditional evaluation techniques and hence cannot be evaluated directly. In order to obtain an analytically tractable expression, a number of simplifications need to be made.

For an excitation laser of  $1.55\mu\text{m}$ , a wavelength located at the centre of the telecomm C-band, the dominant contribution to the sideband spectrum comes from transitions between the highest valence band,  $E_v[\tilde{\mathbf{k}}(t)]$ , and the lowest conduction band,  $E_c[\tilde{\mathbf{k}}(t)]$ . In this region of the Brillouin zone the bands are approximately linear so one can expand the bands to first order about the excitation point  $\mathbf{k}_{ex}$

$$E_c[\tilde{\mathbf{k}}(t)] - E_v[\tilde{\mathbf{k}}(t)] \approx E_g + 2\hbar\tilde{\mathbf{v}}_{f,vc} \cdot (\tilde{\mathbf{k}}(t) - \mathbf{k}_{ex}), \quad (\text{S5})$$

where

$$E_g = E_c[\mathbf{k}_{ex}] - E_v[\mathbf{k}_{ex}], \quad (\text{S6})$$

and

$$\tilde{\mathbf{v}}_{f,vc} = \frac{\hbar v_f^2 \mathbf{k}_{ex} (E_v[\mathbf{k}_{ex}] - E_c[\mathbf{k}_{ex}])}{2E_v[\mathbf{k}_{ex}]E_c[\mathbf{k}_{ex}]} \left[ 1 - \frac{\gamma^2 + V^2}{\sqrt{v_f^2 \mathbf{k}_{ex}^2 (\gamma^2 + V^2) + \gamma^4}} \right]. \quad (\text{S7})$$

For the parameters given in the main text one finds that the effective Fermi velocity is  $|\tilde{\mathbf{v}}_{f,vc}| = 5.90 \frac{eV\text{\AA}}{\hbar}$  (close to the value of  $6.46 \frac{eV\text{\AA}}{\hbar}$  for monolayer graphene). Note that, owing to the rotational symmetry of the bands, the excitation resonance will consist of a circle of radius  $|\mathbf{k}_{ex}|$  centred on the Dirac point. Essentially, the bands look like a shifted version of the mono-layer graphene bands with a modified Fermi velocity given by Eq. (S7).

By substituting the expression in Eq. (S5) into the quasi-classical action in Eq. (S4) and then minimizing it with respect to each variable, one can find the classical equations of motion for the system. For a THz field polarized in the x-direction one finds

$$E_g + 2\tilde{\mathbf{U}}_{p,vc} \cdot \left( \frac{\tilde{\mathbf{k}}(t-\tau) - \mathbf{k}_{ex}}{\alpha} \right) = \hbar\omega_{ex} - i\Gamma, \quad (\text{S8a})$$

$$E_g + 2\tilde{\mathbf{U}}_{p,vc} \cdot \left( \frac{\tilde{\mathbf{k}}(t) - \mathbf{k}_{ex}}{\alpha} \right) - \hbar\omega_{ex} + i\Gamma = \hbar\omega_s, \quad (\text{S8b})$$

$$2\tilde{\mathbf{v}}_{f,vc}\tau = 0, \quad (\text{S8c})$$

where  $\alpha = \frac{e|F_{THz}|}{\hbar\omega_{THz}}$  is the maximum momentum the electron-hole pair can obtain from the THz field,  $\hbar\omega_s = \hbar\omega - \hbar\omega_{ex}$  is the sideband energy centred around the optical excitation frequency and  $\tilde{\mathbf{U}}_{p,vc} = \frac{e\tilde{\mathbf{v}}_{f,vc}|F_{THz}|}{\omega_{THz}}$  is the linear ponderomotive energy associated with particle motion in each of the two coordinate directions. The classical equations give the constraint conditions for a fully classical electron-hole pair to produce sidebands. Equation (S8a) states that the electron-hole pairs are created at time  $t - \tau$  with an energy equal to the excitation

field energy; Eq. (S8b) states that the sideband energy is given by the difference in the energy of the electron-hole pair at time  $t$  and  $t - \tau$ . Equation (S8c) states that the electron-hole pair must be at the same location to recombine, which occurs only when the transit time,  $\tau$ , is zero for linear dispersion bands. This is an indication that the particles behave like massless Dirac particles because, for non-zero transit times, the classical separation grows linearly at twice the Fermi velocity. For classical particles the constraints imposed by Eqs. (S8a-c) cannot be satisfied for non-zero  $\tau$  and hence one would not expect to see sidebands. However, for quantum particles there may be non-vanishing overlap of the electron and hole wavefunctions and hence the particles do not have to be in the same location to recombine. Following [21], we relax the last constraint in Eq. (S8c) and maximise the sideband energy under the conditions of the remaining two. This leads to

$$\hbar\omega_s = 2|\tilde{\mathbf{U}}_{p,vc}|(\sin[\omega_{THz}(t - \tau)] - \sin[\omega_{THz}t]), \quad (\text{S9})$$

which is maximized for  $t = \frac{3\pi}{2}, \tau = \pi$  and minimized for  $t = \frac{\pi}{2}, \tau = \pi$ . Thus, one expects a symmetric plateau about the excitation frequency with cutoffs at  $\pm 4|\tilde{\mathbf{U}}_{p,vc}|$ . The maximum/minimum energy sideband is given by electron-hole pairs that are excited at the point of minimum/maximum THz field and accelerated/decelerated for a half cycle. For electron-hole pairs that travel for longer, the THz field will reverse direction part way through the electron-hole pair's motion decelerating/accelerating the particles resulting in an energy change that is smaller than the maximum.  $4|\tilde{\mathbf{U}}_{p,vc}|$  represents the maximum energy the electron-hole pair can gain or lose via interactions with the THz field.

### **The effect of relaxation on bandwidth**

Equation (S9) give the maximum sideband energy for an electron-hole pair that is created at  $t - \tau$  and recombines at  $t$ . This expression is maximized for  $t = \frac{3\pi}{2}, \tau = \pi$ . Thus, in order to

obtain the maximum modulation the electron-hole pairs must travel for a full half cycle, which, for the 1 THz driving field described in the main text, is 500 fs. For relaxation times greater than half the period of the THz driving field the electron-hole pair can travel for the necessary length of time for the maximum modulation to occur and, hence, one should observe the full sideband plateau. For relaxation times less than half the time period then electron-hole pairs will relax before they can travel for the necessary length of time to achieve maximum modulation and, hence, the plateau should be absent.

Figure S1 shows the effect of the relaxation time on the sideband spectrum of BLG driven by a  $2.5 \text{ kVcm}^{-1}$  strength field with frequency of 1 THz. The half cycle time of 500 fs is shown by the dashed line. Above this line, when the relaxation time is longer than the half-cycle time one sees a prominent plateau. Below the line, when the relaxation time is shorter than the half-cycle time, the plateau strength reduces and for very short relaxation times vanishes completely. Note that by increasing the frequency of the THz field one would reduce the half-cycle time and hence reduces the minimum relaxation required to observe a plateau. However, as the linear ponderomotive energy is inversely proportional to the THz field frequency this would lead to a smaller plateau and subsequently a smaller bandwidth modulation.

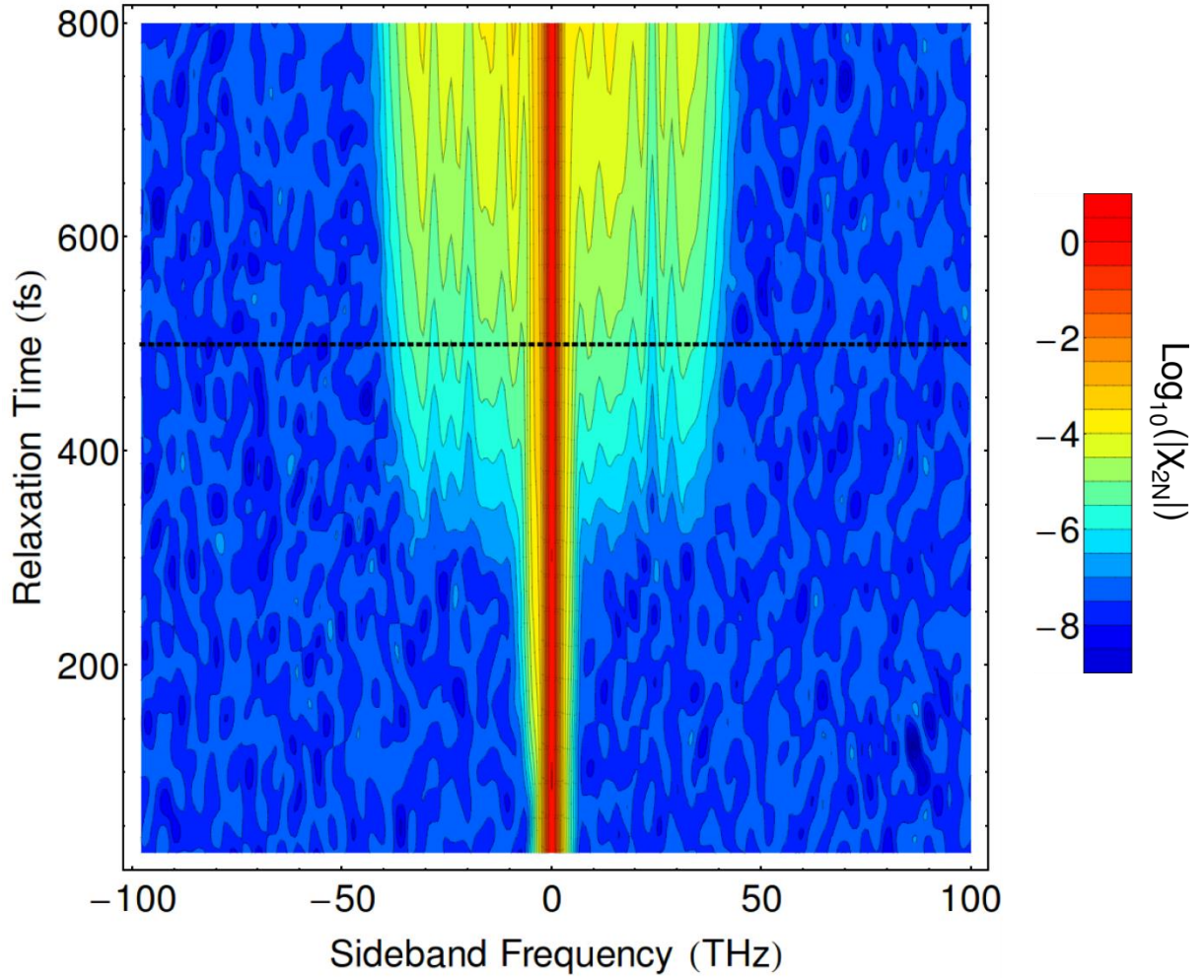


**Figure S1: The effect of relaxation times on the sideband spectrum of a THz driven bi-layer graphene.** Contour plot of the sideband spectrum of THz driven BLG for different relaxation times. The colour map gives the logarithm of the normalized sideband amplitude  $\log_{10}(|\chi_{2N}|)$ . The dashed black line indicates half the THz field period, 500 fs. The strength of the THz field is  $2.5 \text{ kVcm}^{-1}$ .

## Supplementary References

31. Castro Neto, A. H., Guinea, F., Peres, N. M. R., Novoselov, K. S. and Geim, A. K. The electronic properties of graphene. *Rev. Mod. Phys.* **81**, 109 (2009).
32. Das Sarma, S., Adam, S., Hwang, E. H. and Rossi, E. Electronic transport in two-dimensional graphene. *Rev. Mod. Phys.* **83**, 407 (2011).
33. Li, Z. Q., et al. Band structure asymmetry of bi-layer graphene revealed by infrared spectroscopy. *Phys. Rev. Lett.* **102**, 037403 (2009).
34. Novoselov, K. S., et al. Unconventional quantum hall effect and Berry's phase of  $2\pi$  in bilayer graphene. *Nat. Phys.* **2**, 177 (2006).
35. McCann, E. and Falko, V. I. Landau-level degeneracy and quantum hall effect in a graphene bi-layer. *Phys. Rev. Lett.* **96**, 086805 (2006).
36. Yang, F. and Liu, R.-B. Berry phases of quantum trajectories of optically excited electron-hole pairs in semiconductors under strong terahertz fields, *New J. Phys.* **15**, 115005 (2013).
37. Yan, J.-Y. Theory of excitonic high-order sideband generation in semiconductors under a strong terahertz field. *Phys. Rev. B* **78**, 075204 (2008).